

Far-infrared observation of the electric-dipole spin resonance of donor electrons in $\text{Cd}_{1-x}\text{Mn}_x\text{Se}$

M. Dobrowolska,* A. Witowski,[†] and J. K. Furdyna

Department of Physics, Purdue University, West Lafayette, Indiana 47907

T. Ichiguchi and H. D. Drew

Department of Physics and Astronomy, University of Maryland, College Park, Maryland 20742

P. A. Wolff

Francis Bitter National Magnet Laboratory, Massachusetts Institute of Technology, Cambridge, Massachusetts 02139

(Received 12 January 1984)

Far-infrared (FIR) measurements of electric-dipole spin resonance (EDSR) of donor-bound electrons in $\text{Cd}_{1-x}\text{Mn}_x\text{Se}$ ($x=0.10$ and 0.20) are reported. The EDSR transition is allowed in $\text{Cd}_{1-x}\text{Mn}_x\text{Se}$ by the combined effects of spin-orbit interaction and the acentric uniaxial symmetry of this wurtzite system. The far-infrared EDSR is observed at magnetic fields of the order of 1 T, indicating extremely large effective g factors (in excess of 100) due to contributions from the exchange interaction between the band electrons and the localized magnetic moments. Measurements as a function of temperature and frequency reveal a strong temperature dependence of the g -factors, and a dramatic increase in the strength of EDSR with frequency. Studies with linear and circular polarization were used to determine the selection rules governing EDSR, as well as the sign of the exchange integral for the conduction band of $\text{Cd}_{1-x}\text{Mn}_x\text{Se}$. EDSR is observed only in samples characterized by low resistivities ($\sim 1 \Omega \text{ cm}$ at 77 K), with donor concentrations in the range of 10^{16} cm^{-3} . In addition to EDSR, the FIR magnetotransmission spectra show several other interesting features, which are interpreted in terms of conduction-electron cyclotron resonance and magnetic field dependence in the $1s \rightarrow 2p$ transitions of the donor levels.

I. INTRODUCTION

We report the observation and detailed investigation of very strong electric-dipole-induced spin resonance (EDSR) of donor-bound electrons in $\text{Cd}_{1-x}\text{Mn}_x\text{Se}$ at far-infrared (FIR) frequencies.¹ The study of this spin-flip transition is motivated by several considerations.

First, as is well known, direct (one-photon) transitions between two spin states are normally forbidden by electric-dipole selection rules. However, in uniaxial acentric crystals (such as the wurtzite systems CdS, CdSe, or $\text{Cd}_{1-x}\text{Mn}_x\text{Se}$) with spin-orbit interaction, electron states are described by a Hamiltonian

$$H = H_0 + H', \quad (1)$$

where H_0 is the unperturbed Hamiltonian, which in the effective-mass approximation can be written as

$$H_0 = \frac{\hbar^2}{2m^*} k^2 - \frac{e^2}{\kappa r} + g\mu_B \vec{s} \cdot \vec{B}, \quad (2)$$

and the perturbation term H' has the form²

$$H' = \lambda[\hat{c} \cdot (\vec{s} \times \vec{k})]. \quad (3)$$

Here \hat{c} is the unit vector along the c axis, \vec{s} and \vec{k} are the spin and momentum operators of the electron, respectively, λ is a constant, m^* and g are the effective mass and the g factor of the electron, respectively, κ is the static

dielectric constant, μ_B is the Bohr magneton, and \vec{B} is the magnetic field. As will be shown below, the effect of Eq. (3) is to admix a contribution from $2p$ and higher *spin-down* states into the wave function of the $1s$ spin-up level, thus allowing electric-dipole-excited spin-flip transitions between $|1s, \downarrow\rangle$, and $|1s, \uparrow\rangle$.

Second, it will also be shown that, since EDSR is made possible by admixing contributions from $|2p, \downarrow\rangle$ states into the $|1s, \uparrow\rangle$ level, the *strength* of EDSR depends critically on the energy separation between the $|2p, \downarrow\rangle$ and $|1s, \uparrow\rangle$ levels. Now, $\text{Cd}_{1-x}\text{Mn}_x\text{Se}$ is a diluted magnetic semiconductor in which the spin splitting of donor levels is dramatically enhanced (by some 2 orders of magnitude compared to CdSe) through exchange interaction between the localized magnetic moments (in this case Mn^{2+}) and band electrons.³ It is this exchange-enhanced spin splitting in $\text{Cd}_{1-x}\text{Mn}_x\text{Se}$ which makes it possible for the $|1s, \uparrow\rangle$ level to approach (and even to cross) the $|2p, \downarrow\rangle$ and higher spin-down levels at fields of the order of 1 T, making the EDSR unusually strong (and therefore experimentally observable) under ordinary laboratory conditions. In nonmagnetic semiconductors such as CdSe the observation of EDSR of comparable strength would require magnetic fields in the megagauss range.

Furthermore, it is also important to note that the physics of the spin splitting of electronic levels in a diluted magnetic semiconductor such as $\text{Cd}_{1-x}\text{Mn}_x\text{Se}$ is extremely interesting in its own right. Spin splitting in these ma-

terials can be described by an effective g factor which, in addition to being anomalously large, is temperature and magnetic field dependent, as has been demonstrated by spin-flip Raman scattering experiments in $\text{Cd}_{1-x}\text{Mn}_x\text{Se}$.^{4,5} The Raman work has also shown that in diluted magnetic semiconductors the spin splitting of donor states does not vanish even at zero magnetic field, because of the bound magnetic polaron.⁴⁻⁶ By providing a direct experimental measurement of this magnetic splitting, far-infrared EDSR constitutes an excellent tool for probing exchange-related phenomena in $\text{Cd}_{1-x}\text{Mn}_x\text{Se}$, including the temperature dependence of the effective g factor, its *sign*, and other features characterizing a diluted magnetic semiconductor.

In addition, in all samples displaying EDSR we have also systematically observed several prominent features in the FIR transmission at magnetic fields away from the EDSR line. Although this aspect of the investigation is to be regarded as preliminary, we find that some features of the data can be explained both in terms of conduction-electron cyclotron resonance and the magnetic field dependence of the $1s \rightarrow 2p$ transition.

This paper is organized as follows. In Sec. II we formulate the matrix elements and selection rules for the electric-dipole transitions which arise as a consequence of Eq. (3). In Sec. III we describe the details of the experimental procedure. Finally, in Sec. IV, we discuss the results of the EDSR experiments, including the temperature and frequency dependence of this spin-flip transition, polarization selection rules, the sign of the exchange integral, and the value of the parameter λ in Eq. (3). In Sec. IV we also describe the behavior of the transmission background away from EDSR, along with a brief discussion of possible mechanisms responsible for the observed behavior.

II. THEORY

Direct transitions between two spin states in the $1s$ level of a hydrogen donor in a semiconductor are forbidden by electric-dipole selection rules. However, when spin-orbit interaction is present, these selection rules can be relaxed by two mechanisms: wave-function mixing through the $\vec{k} \cdot \vec{p}$ interaction (sometimes called the "nonparabolicity" mechanism),^{7,8} or by inversion asymmetry,^{9,10} as a result of which the spin-orbit divergence of the bands appears already in the first order in k . The nonparabolicity mechanism is of little consequence for large-band-gap semiconductors such as $\text{Cd}_{1-x}\text{Mn}_x\text{Se}$ considered in this paper. The influence of inversion asymmetry on spin-flip transitions, on the other hand, is particularly prominent in acentric uniaxial crystals, such as the wurtzite crystals CdS , CdSe , or $\text{Cd}_{1-x}\text{Mn}_x\text{Se}$. As already pointed out, in these materials the Hamiltonian describing electron states contains a term given by Eq. (3). This term, regarded as a perturbation, mixes states of different orbital angular momentum with respect to the \hat{c} axis, but conserves total (orbital plus spin) angular momentum about that axis. Thus the perturbed conduction-band states (which also

describe shallow donors) contain a mixture of "up" and "down" spins, which, in turn, permits the electric-dipole spin-resonance (EDSR) transition either for the conduction or for the donor-bound electrons. The resulting absorption then provides a direct means of determining λ .

In discussing EDSR for $\text{Cd}_{1-x}\text{Mn}_x\text{Se}$, we will assume that the electrons in question are bound in donor states. The ground-state ($1s$) wave functions will be calculated using first-order perturbation theory with H' of Eq. (3) as the perturbing Hamiltonian. For clarity, we will consider separately two distinct geometries which occur in our experiments, $\vec{B} \parallel \hat{c}$ and $\vec{B} \perp \hat{c}$, where \vec{B} is the dc magnetic field.

A. $\vec{B} \parallel \hat{c}$ geometry

In the $\vec{B} \parallel \hat{c}$ geometry the linear- k perturbation H' takes the form

$$H' = \lambda(s_x k_y - s_y k_x), \quad (4)$$

where we have chosen the coordinates such that $\vec{B} \parallel \hat{z}$ and $\hat{c} \parallel \hat{z}$. Rewriting Eq. (4) in terms of raising and lowering operators, we can now immediately determine the effect of the operator H' on the $1s$ donor levels,

$$\begin{aligned} H' |1s, \uparrow\rangle &= \frac{\lambda}{2i} [(s_x - is_y)(k_x + ik_y) \\ &\quad - (s_x + is_y)(k_x - ik_y)] |1s, \uparrow\rangle \\ &= -\frac{\lambda}{2} \left[\frac{\partial}{\partial x} + i \frac{\partial}{\partial y} \right] |1s, \downarrow\rangle \\ &= \left[\frac{\lambda}{2a_0^*} \right] \sin(\theta) e^{i\phi} |1s, \downarrow\rangle, \end{aligned} \quad (5)$$

where a_0^* is the effective Bohr radius of the donor state. Here and in what follows we are considering the low-magnetic-field limit, i.e., a_0^* much smaller than the magnetic length $l_0 = (eH/\hbar c)^{-1/2}$. This condition is reasonably satisfied in our experiments.

First-order perturbation theory then gives the wave function for the $1s$ donor level in the form

$$\psi_{1s, \uparrow} = |1s, \uparrow\rangle + \sum_{\alpha} \frac{|\alpha\rangle \langle \alpha | H' | 1s, \uparrow \rangle}{E(1s, \uparrow) - E(\alpha)}, \quad (6)$$

where α labels all other states admixing into $|1s, \uparrow\rangle$. By inspection of Eq. (5) it is readily seen that the only nonvanishing contribution to the sum in Eq. (6) will come from $\alpha = (np^+, \downarrow)$ (i.e., from p states with the magnetic quantum number $m = +1$ and spin \downarrow). Equation (6) can thus be written

$$\psi_{1s, \uparrow} = |1s, \uparrow\rangle - \frac{i\lambda}{2\hbar} \sum \frac{|np^+, \downarrow\rangle \langle np^+, \downarrow | p_x + ip_y | 1s, \downarrow \rangle}{E(1s, \uparrow) - E(np^+, \downarrow)}, \quad (7)$$

where the summation is over all principal quantum numbers $n \geq 2$, as well as states in the continuum.

Using the unperturbed Hamiltonian H_0 , Eq. (2), we obtain the relation between the momentum and position matrix elements

$$\langle np^+, \downarrow | p_x + ip_y | 1s, \downarrow \rangle = \frac{im^*}{\hbar} \left[E(np^+, \downarrow) - E(1s, \downarrow) - \mu_B B \frac{m_e}{m^*} \right] \langle np^+, \downarrow | x + iy | 1s, \downarrow \rangle, \quad (8)$$

where m_e is the free-electron mass. We can thus rewrite Eq. (7) as

$$\psi_{1s, \uparrow} = |1s, \uparrow\rangle - \frac{\lambda m^*}{2\hbar^2} \sum \frac{E(1s, \downarrow) - E(np^+, \downarrow) + \mu_B B m_e/m^*}{E(1s, \uparrow) - E(np^+, \downarrow)} |np^+, \downarrow\rangle \langle np^+, \downarrow | x + iy | 1s, \downarrow \rangle. \quad (9)$$

Assuming that the spin splitting of the ground and excited states are the same, we can write the eigenvalues of H_0 appearing in Eqs. (7)–(9) in the standard form,

$$E_{nlmm_s} = -\frac{m^* e^4}{2\kappa^2 \hbar^2} \frac{1}{n^2} + \mu_B B \left[gm_s + \frac{m_e}{m^*} m \right] = E_{nl} + \mu_B B \left[gm_s + \frac{m_e}{m^*} m \right], \quad (10)$$

where $m = \pm 1, 0$ and $m_s = +\frac{1}{2}$ or $-\frac{1}{2}$, corresponding to spins \uparrow or \downarrow , respectively. In Eq. (9) only the $m = +1$ term contributes to the sum. Owing to the large value of g in diluted magnetic semiconductors (see below), in what follows we will ignore, for the moment, the last term in Eq. (10) compared to the spin-splitting contribution $m_s g \mu_B B$. We then have

$$\psi_{1s, \uparrow} = |1s, \uparrow\rangle - \frac{\lambda m^*}{2\hbar^2} \sum \frac{(E_{np} - E_{1s}) |np^+, \downarrow\rangle \langle np^+, \downarrow | x + iy | 1s, \downarrow \rangle}{E_{np} - E_{1s} - \hbar\omega_s}, \quad (11)$$

where E_{np} and E_{1s} are the donor levels for $B=0$, and $\hbar\omega_s = g\mu_B B$. Because—in comparison with the $1s$ level—all excited states lie rather close together, we will replace the difference $E_{np} - E_{1s}$ in Eq. (11) by an average effective excitation energy ΔE , independent of n . The value of ΔE is expected to be somewhat—but not much—larger than the $1s \rightarrow 2p$ excitation energy. Summation over the complete set of eigenstates of H_0 then gives

$$\psi_{1s, \uparrow} \simeq |1s, \uparrow\rangle - \frac{\lambda m^*}{2\hbar^2} \frac{\Delta E}{\Delta E - \hbar\omega_s} (x + iy) |1s, \downarrow\rangle. \quad (12)$$

Similarly, the wave function for the $(1s, \downarrow)$ state is found to be

$$\psi_{1s, \downarrow} \simeq |1s, \downarrow\rangle + \frac{\lambda m^*}{2\hbar^2} \frac{\Delta E}{\Delta E + \hbar\omega_s} (x - iy) |1s, \uparrow\rangle. \quad (13)$$

Using Eqs. (12) and (13), one can now obtain the EDSR matrix element for $\vec{B} \parallel \hat{z}$. For this geometry the matrix element has a finite value for one circular polarization,

$$\langle \psi_{1s, \uparrow} | \hat{e}_+ \cdot \vec{r} | \psi_{1s, \downarrow} \rangle = -\frac{\lambda}{\sqrt{2}R^*} \frac{\Delta E \hbar\omega_s}{\Delta E^2 - \hbar^2 \omega_s^2}, \quad (14)$$

where R^* is the effective Rydberg constant, and \hat{e}_+ is the unit vector designating the polarization of incident light,

$$\hat{e}_+ = (\hat{x} + i\hat{y})/\sqrt{2}.$$

For the opposite sign of circular polarization, and for linear polarization $\vec{E} \parallel \vec{B}$, the EDSR matrix element vanishes. Which circular polarization induces EDSR depends on whether the energy of the $|1s, \downarrow\rangle$ state lies below or above the $|1s, \uparrow\rangle$ energy. When $E(1s, \downarrow) < E(1s, \uparrow)$ (i.e., when the spin splitting is described by a *positive* g factor), the circular polarization producing EDSR is the same as that which excites cyclotron resonance of free electrons. We shall refer to this polarization as cyclotron-resonance-active (CRA). When the situation is reversed [$E(1s, \downarrow) > E(1s, \uparrow)$, i.e., the g factor is *negative*], the EDSR is excited only by the cyclotron-resonance-inactive

polarization (CRI). This identification will be important for determining the sign of the g factor in Sec. IV.

The form of the denominator of Eq. (14) is a consequence of the fact that the $|1s, \uparrow\rangle$ and $|np^+, \downarrow\rangle$ levels are approaching each other, while $|1s, \downarrow\rangle$ and $|np^-, \uparrow\rangle$ are moving further apart as the field increases, altering the amount of p -state admixture into the ground donor state.

B. $\vec{B} \perp \hat{z}$ geometry.

Next, we consider the second configuration, $\vec{B} \perp \hat{z}$. Taking $\vec{B} \parallel \hat{y}$ and $\hat{z} \parallel \hat{x}$, the perturbation Hamiltonian (3) has the form

$$H' = \lambda(s_y k_z - s_z k_y). \quad (15)$$

Proceeding as before, we now obtain

$$\psi_{1s, \uparrow} \simeq \left[1 + \frac{i\lambda m^*}{2\hbar^2} y \right] |1s, \uparrow\rangle + \frac{\lambda m^*}{2\hbar^2} \frac{\Delta E}{\Delta E - \hbar\omega_s} z |1s, \downarrow\rangle, \quad (16)$$

$$\psi_{1s, \downarrow} \simeq \left[1 - \frac{i\lambda m^*}{2\hbar^2} y \right] |1s, \downarrow\rangle - \frac{\lambda m^*}{2\hbar^2} \frac{\Delta E}{\Delta E + \hbar\omega_s} z |1s, \uparrow\rangle. \quad (17)$$

The EDSR matrix element in this case has only a \hat{z} component, i.e., it is excited by an electric field polarized parallel to the dc magnetic field. Equations (16) and (17) then lead to a matrix element for the spin flip transition,

$$\langle \psi_{1s, \uparrow} | z | \psi_{1s, \downarrow} \rangle = \frac{\lambda}{2R^*} \frac{\Delta E \hbar\omega_s}{\Delta E^2 - \hbar^2 \omega_s^2}. \quad (18)$$

C. Selection rules and absorption coefficient

The results in subsections A and B lead to the following selection rules.

(a) Case $\vec{B} \parallel \hat{z}$: EDSR is excited only by $\vec{E} \perp \vec{B}$. Furthermore, only one sign of circular polarization [see discus-

sion following Eq. (14) is active in exciting the spin-flip transition.

(b) Case $\vec{B} \perp \hat{c}$: EDSR is excited only by $\vec{E} \parallel \vec{B}$.

Finally, in order to compare these results to experiment, we relate the matrix element for EDSR to a corresponding absorption coefficient α_{EDSR} in the standard manner, through the imaginary part of the dielectric function $\epsilon''(\omega)$,

$$\alpha_{\text{EDSR}} = \frac{\omega \epsilon''(\omega)}{cn} = \frac{8\pi\omega^2}{\hbar cn} \frac{Ne^2\omega_s \Gamma}{(\omega_s^2 - \omega^2)^2 + \Gamma^2\omega^2} |X|^2. \quad (19)$$

Here N is the donor concentration, Γ is the full width at half-height, n is the refractive index, and $|X|$ is the matrix element given by Eqs. (14) or (18), depending on the experimental configuration. Thus at $\omega = \omega_s$ the absorption coefficient takes the form

$$[\alpha_{\text{EDSR}}]_{\omega=\omega_s} = \frac{8\pi\omega Ne^2 |X|^2}{\hbar cn \Gamma}. \quad (20)$$

For $\vec{B} \parallel \hat{c}$ and $\vec{E} \perp \vec{B}$, substituting Eq. (14) for $|X|$, we obtain an explicit form for the absorption coefficient at EDSR,

$$[\alpha_{\text{EDSR}}]_{\omega=\omega_s} = \frac{4\pi\hbar\omega^3 Ne^2 \lambda^2}{cn \Gamma R^{*2}} \left[\frac{\Delta E}{\Delta E^2 - \hbar^2 \omega_s^2} \right]^2, \quad (21)$$

and a similar expression [one-half of Eq. (21)] for the $\vec{B} \perp \hat{c}$ and $\vec{E} \parallel \vec{B}$ geometry.

It is important to recall that in diluted magnetic semiconductors such as $\text{Cd}_{1-x}\text{Mn}_x\text{Se}$ the value of $\hbar\omega_s$ can be of the order of ΔE (i.e., 10–20 meV) in normal laboratory magnetic fields (for instance, at 1 T). This leads to values of α which in nonmagnetic semiconductors (such as CdSe) could only be satisfied at megagauss fields. This feature illustrates the *magnetic field enhancement* by exchange interaction characteristic of diluted magnetic semiconductors. Thus the integrated intensity $\alpha\Gamma$ of EDSR has a very sensitive frequency dependence: an ω^3 dependence arising explicitly from the numerator of Eq. (21) and, in addition, a resonant behavior ensuing from the denominator of $|X|$, which becomes extremely important when $\hbar\omega$ approaches ΔE .

Finally, for comparison with the donor EDSR, we also consider the EDSR of electrons in the conduction band. In that case the perturbation Hamiltonian (3) mixes the spin states of the adjacent Landau levels. For example, for the $\vec{B} \parallel \hat{c}$ Faraday geometry, the $|\nu+1, \downarrow\rangle$ state is ad-

mixed to the $|\nu, \uparrow\rangle$ state (where ν designates the Landau-level quantum number), permitting the EDSR transition ($\nu, \downarrow \rightarrow \nu, \uparrow$). The resulting absorption coefficient for the allowed polarization (CRA when the g factor is positive) is calculated to be

$$[\alpha_{\text{EDSR}}]_{\omega=\omega_s} = \frac{4\pi Ne^2 \lambda^2}{\hbar^3 \omega cn \Gamma} \frac{\omega_s^2}{(\omega_c - \omega_s)^2}, \quad (22)$$

where N is the conduction-electron density and ω_c is the cyclotron frequency. For this free-carrier case the integrated intensity $\alpha\Gamma$ is seen to be proportional to ω^{-1} , in distinct contrast to the donor case above. As will be seen later, the sharp increase of EDSR intensity with frequency observed at liquid-helium temperatures closely follows the behavior predicted by Eq. (21), providing strong support to the assumption that low-temperature EDSR is taking place on donor-bound electrons.

II. EXPERIMENT

The $\text{Cd}_{1-x}\text{Mn}_x\text{Se}$ crystals used in these experiments were grown from the melt by the Bridgman method. The composition of the samples was determined by electron-microprobe analysis, which in all cases examined was very close to the composition of starting materials used in growing the crystal.

The EDSR was observed in samples cut from three different ingots of $\text{Cd}_{1-x}\text{Mn}_x\text{Se}$, two with $x \simeq 0.1$ and one with $x \simeq 0.2$. All three ingots showed low resistivities (below 1 Ω cm) and a high electron concentration (typically $n \simeq 10^{16}$ cm^{-3}) at 77 K, with little change between 77 K and room temperature. This indicates the presence of approximately 10^{16} cm^{-3} donors in the specimens. The origin of the donors has not been identified. Since the ingots were not intentionally doped, the donors may result from defects associated with nonstoichiometry, common in II-VI compounds. However, the presence of an accidental impurity has not been conclusively eliminated.

The electron concentration, resistivity, and mobility for the $\text{Cd}_{1-x}\text{Mn}_x\text{Se}$ ingots used in the EDSR measurements, obtained by the van der Pauw method, are collected in Table I. The values of x indicated in the table are the electron-microprobe results.

Detailed transport measurements were also performed on a sample from ingot *A* at low temperatures. Briefly, the sample resistivity increases to over 10^4 Ω cm at 4.2 K and shows a rather dramatic negative magnetoresistance,¹¹

TABLE I. Electrical properties of $\text{Cd}_{1-x}\text{Mn}_x\text{Se}$ samples.

Temperature and properties	Ingot designation: Mn concentration:	<i>A</i>	<i>B</i>	<i>C</i>
		$x=0.10$	$x=0.097$	$x=0.22$
$T=236$ K	ρ (Ω cm)	0.83	0.62	0.69
	μ_n ($\text{cm}^2/\text{V sec}$)	370	510	420
	n (cm^{-3})	2.0×10^{16}	2.0×10^{16}	2.0×10^{16}
$T=77$ K	ρ (Ω cm)	0.37	0.32	0.34
	μ_n ($\text{cm}^2/\text{V sec}$)	1410	1820	1870
	n (cm^{-3})	1.2×10^{16}	1.1×10^{16}	9.9×10^{15}

similar to that previously observed by others.¹²

We have also carried out FIR magnetotransmission measurements on several $\text{Cd}_{1-x}\text{Mn}_x\text{Se}$ samples having high resistivity (of the order of $10^4 \Omega \text{ cm}$ or higher at 77 K). All such samples were much more transparent to FIR than those cut from ingots *A*, *B*, and *C*, and none showed EDSR or any of the other FIR magnetotransmission features mentioned earlier.

The far-infrared magnetotransmission experiments were carried out on two different experimental setups (at Purdue University and at the University of Maryland), giving identical—and very reproducible—results. The FIR radiation was generated by either an optically pumped or by an electrical-discharge FIR laser, and measurements were performed at a series of fixed wavelengths between 96.5 and 337 μm , in the temperature range between 2 and 35 K, and in magnetic fields up to 8 T. We used oriented single-crystal specimens in the form of plane parallel slabs, about 1 mm thick, oriented with the *c* axis either in the plane of the sample or normal to the sample face. The experiments were performed in both Voigt and Faraday geometries. Measurements in the Faraday configuration were carried out using either unpolarized or circularly polarized incident FIR. In the Voigt geometry, linear incident polarization was used, either parallel or perpendicular to \vec{B} .

IV. RESULTS

A. Electric-dipole spin resonance

Magnetotransmission spectra observed at 4.2 K on a sample with $x=0.1$ (ingot *A*) in the Faraday geometry

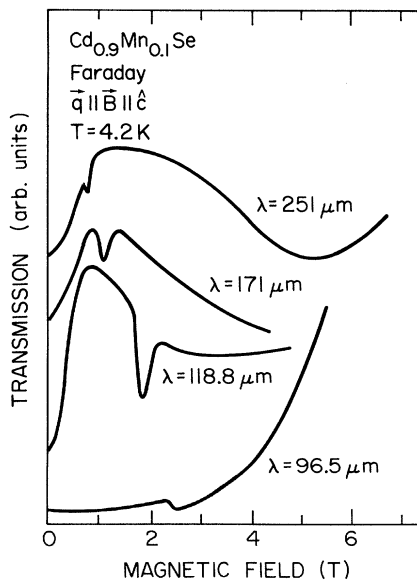


FIG. 1. Magnetic field and frequency dependence of magnetotransmission in $\text{Cd}_{0.9}\text{Mn}_{0.1}\text{Se}$ (ingot *A*) at 4.2 K for unpolarized FIR in the Faraday geometry. The *c* axis is normal to the face of the sample. EDSR is clearly seen as the prominent absorption dip, superimposed on the slowly varying magnetic-field-dependent background.

($\vec{q} \parallel \vec{B} \parallel \hat{c}$), using unpolarized incident FIR, are shown in Fig. 1 for several wavelengths. The most striking feature of the data is the single well-defined resonance line, which we identify as the EDSR transition of electrons in the $1s$ donor level. Another characteristic feature clearly shown in Fig. 1—and common to all samples exhibiting EDSR—is that the resonance line occurs on a strongly magnetic-field-dependent background. The third feature we would like to point out is the broad dip in the 251- μm data, seen in Fig. 1 at about 5.2 T, which we attribute to free-carrier cyclotron resonance. We will return to these features of the transmission background at the end of the paper.

Figure 2 presents magnetotransmission spectra observed at 4.5 K in a sample with $x=0.2$ (ingot *C*), with the *c* axis parallel to the sample plane. The data were taken at two wavelengths (118.8 and 96.5 μm), using linear polarization in the perpendicular Voigt geometry ($\vec{B} \parallel \hat{c} \perp \vec{E}$). As in Fig. 1, the EDSR line is superimposed on a varying background and shifts to higher fields as the frequency increases.

Figure 3 shows the magnetic field dependence of the EDSR energy observed on samples with $x=0.10$ (ingots *A* and *B*) at several fixed temperatures. At higher temperatures ($T \geq 10$ K) the EDSR splits into a doublet. The lower- and higher-field positions of the doublet are shown as solid and open circles, respectively.

The results are compared with the energies of the spin-flip Raman lines observed by Heiman *et al.*,⁵ who performed their measurements on samples with $x=0.1$ taken from the same ingot *A* as one of our samples (see Table I). The Raman data for $T=4.6$ and 19 K are presented as dashed lines. The EDSR and Raman data are in good agreement, as would be expected, since the two phenomena involve the same spin-flip transition.

An important feature of EDSR in $\text{Cd}_{1-x}\text{Mn}_x\text{Se}$ is its

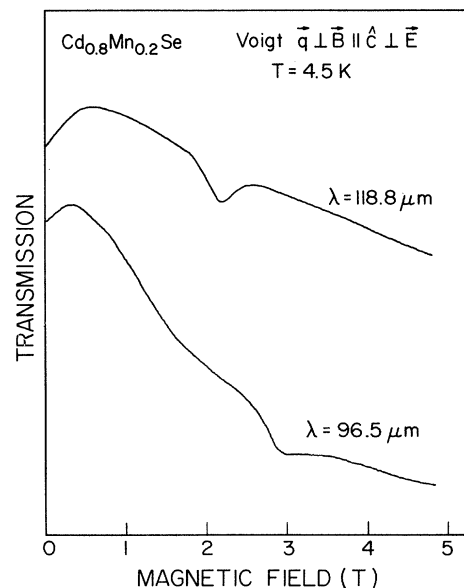


FIG. 2. Magnetotransmission in $\text{Cd}_{0.8}\text{Mn}_{0.2}\text{Se}$ (ingot *C*) at 4.5 K in the perpendicular Voigt geometry for two FIR frequencies. The *c* axis is in the face of the sample.

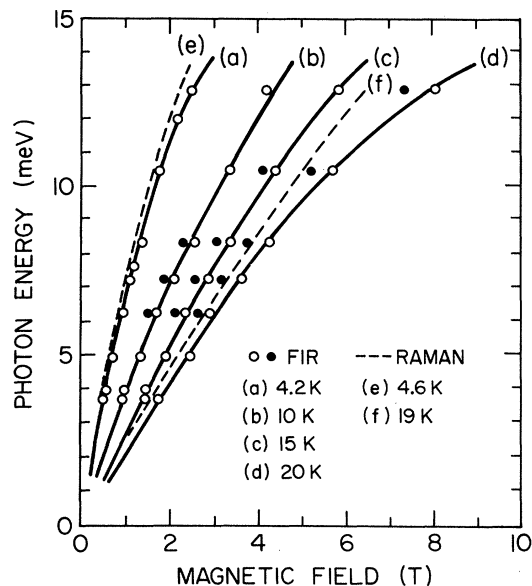


FIG. 3. Magnetic field dependence of the EDSR energy for $\text{Cd}_{0.9}\text{Mn}_{0.1}\text{Se}$ as a function of temperature. Solid and open circles show the doublet structure observed at high temperature, the solid circles corresponding to the new line which emerges above 10 K and grows stronger as the temperature continues to increase. The dashed lines are the Raman spin-flip scattering taken from Ref. 5.

temperature dependence, shown in Fig. 4, which can be understood as follows. The Zeeman splitting can be described by an effective g factor which, in a diluted magnetic semiconductor such as $\text{Cd}_{1-x}\text{Mn}_x\text{Se}$, can be written in the form³

$$g_{\text{eff}} = g^* + \frac{N_s \alpha \langle S_z \rangle}{\mu_B H} = g^* - \frac{\alpha M}{g_{\text{Mn}} \mu_B^2 H}, \quad (23)$$

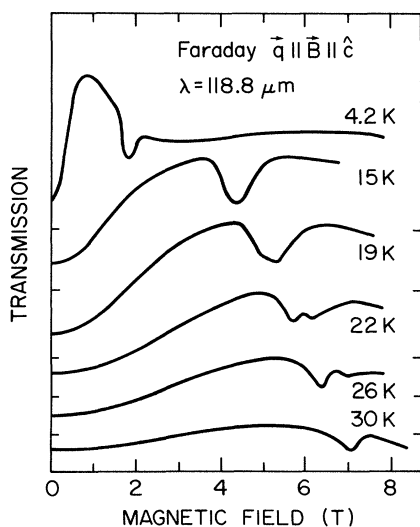


FIG. 4. FIR magnetotransmission in $\text{Cd}_{0.9}\text{Mn}_{0.1}\text{Se}$ (ingot A; same sample as in Fig. 1) in the Faraday configuration at several temperatures. As the temperature increases above 10 K, a new line appears on the low-field side of the original resonance and grows in intensity.

where g^* is the g factor as determined by band parameters of $\text{Cd}_{1-x}\text{Mn}_x\text{Se}$ alone (i.e., in the absence of exchange interaction), $\alpha \equiv \langle S | J | S \rangle / \Omega_0$ is the exchange integral, N_s is the number of Mn^{2+} ions per unit volume, M is the dc magnetization, g_{Mn} is the g factor for Mn^{2+} ions ($g_{\text{Mn}} = 2.0$), and μ_B is the Bohr magneton. The last term is dominant and varies with temperature (and B) as the magnetization of the sample. Thus, for a fixed wavelength, the resonance moves to higher fields as the temperature increases, because the magnetization decreases. The effective g factor itself is very large, having, e.g., a value of 115 at 4.2 K, and it decreases rapidly with rising temperature, as can be seen from Fig. 4.

This figure also shows the splitting of EDSR at higher temperatures, $T \geq 10$ K. The splitting is seen for $\hbar\omega > 6$ meV and it corresponds to a new line (solid circles in Fig. 3) appearing on the low-field side of the resonance. This lower-field EDSR line becomes dominant at higher temperatures. The origin of the new line is not understood at present. It is possible that this line corresponds to EDSR of conduction electrons being excited by the increasing temperature. We note in this regard that in InSb the g factors of donor-bound and conduction electrons are slightly different, giving rise to a similar pair of lines.¹³ However, a more systematic study of this high-temperature line—including the frequency dependence of its intensity—will be required to support or exclude this possibility.

When the magnetization is far from saturation ($\hbar\omega \ll E_{\text{sat}} = 26$ meV; see Ref. 5), Eq. (23) can be approximated by³

$$g_{\text{eff}} = g^* - \frac{35}{12} \frac{N_s^* \alpha g_{\text{Mn}}}{k_B (T + T_{\text{AF}})}, \quad (24)$$

where N_s^* is the effective Mn^{2+} -ion density (which is smaller than N_s), and T_{AF} is an effective Weiss temperature.⁵ Both of these modifications to the Curie law are due to antiferromagnetic (AF) interactions between the Mn^{2+} ions. Therefore, for small g^* (in our case, g^* is not more than 2.0), g_{eff} is proportional to $(T + T_{\text{AF}})^{-1}$. The experimental value of g_{eff} can be obtained from the slope of the spin-resonance frequency versus magnetic field (Fig. 3) in the range of photon energies $3.5 < \hbar\omega < 7.25$ meV, where the curves are reasonably linear. In this range we have $E_{\text{BMP}} \ll \hbar\omega \ll E_{\text{sat}}$ (where E_{BMP} is the zero-field splitting due to the bound magnetic polaron⁵), so that Eq. (24) should adequately describe the EDSR position. In Fig. 3 we see that the EDSR appears to be saturating at a lower energy than is observed in the Raman data. In fact, we are probably seeing the breakdown in the line-shape theory due to the near degeneracy of the $|1s, \uparrow\rangle$ and the $|2p^+, \downarrow\rangle$ donor states as $\hbar\omega$ approaches 15 meV. These states, which are coupled by the linear k perturbation [Eq. (3)], should exhibit the usual degenerate perturbation-theory mode-repulsion effects for $\hbar\omega_s = E_{2p^+} - E_{1s}$. Figure 5 shows the temperature dependence of g_{eff}^{-1} , which is seen to be accurately proportional to $T + T_{\text{AF}}$, with $T_{\text{AF}} \approx 2.7$ K. This agrees well with the Raman experiments by Heiman *et al.*⁵ (dotted line in Fig. 5). The slope of Fig. 5 yields the value $N_s^* \alpha = (-11.9 \pm 1.0)$ meV.

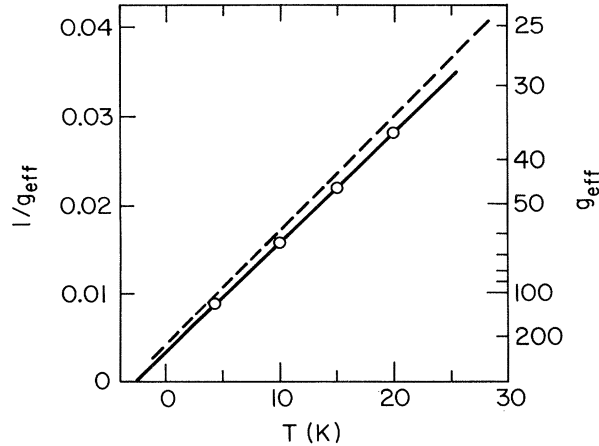


FIG. 5. Temperature dependence of g_{eff}^{-1} obtained from EDSR (open circles in Fig. 3). The dashed line represents the Raman scattering results from Ref. 5.

Selection rules for EDSR were determined by transmission of polarized FIR in various configurations involving the relative orientations of \vec{B} , \hat{c} , and the electric field \vec{E} of the wave. Table II summarizes the EDSR experiments with linear polarization.

There are five independent configurations involving mutual combinations of vectors \vec{B} , \vec{E} , and \hat{c} , identified in the first column in the table. These configurations can be achieved in eight distinct experimental geometries. For example, $\vec{B} \parallel \hat{c}$ and $\vec{E} \perp \hat{c}$ are satisfied in the Faraday geometry for $\vec{q} \parallel \hat{c}$ (where \hat{q} is the wave vector of the propagating FIR), and also in the perpendicular Voigt geometry ($\vec{E} \perp \vec{B}$) when the c axis is in the face of the sample ($\vec{q} \perp \hat{c}$) and \vec{B} is along the c axis. The results collected in Table II can be summarized in the following simple statement: The EDSR transition is observed only when

$$\vec{B} \times (\vec{E} \times \hat{c}) \neq 0. \quad (25)$$

TABLE II. Selection rules for EDSR.

Field configuration	Experimental geometry	EDSR observed
$\vec{B} \parallel \hat{c}, \vec{E} \perp \hat{c}$	$\vec{q} \parallel \hat{c}$, Faraday $\vec{q} \perp \hat{c}, \vec{B} \parallel \hat{c}$, Voigt $\vec{E} \perp \vec{B}$	Yes
$\vec{B} \perp \hat{c}, \vec{E} \parallel \vec{B}$	$\vec{q} \parallel \hat{c}$, Voigt $\vec{E} \parallel \vec{B}$ $\vec{q} \perp \hat{c}, B \perp \hat{c}$, Voigt $\vec{E} \parallel \vec{B}$	Yes
$\vec{B} \perp \hat{c}, \vec{E} \perp \vec{B}, \vec{E} \perp \hat{c}$	$\vec{q} \parallel \hat{c}$, Voigt $\vec{E} \perp \vec{B}$ $\vec{q} \perp \hat{c}$, Faraday	No
$\vec{E} \parallel \hat{c}, \vec{B} \perp \hat{c}$	$\vec{q} \perp \hat{c}, \vec{B} \perp \hat{c}$, Voigt $\vec{E} \perp \vec{B}$ $\vec{q} \perp \hat{c}$, Faraday	No
$\vec{E} \parallel \hat{c}, \vec{B} \parallel \hat{c}$	$\vec{q} \perp \hat{c}, \vec{B} \parallel \hat{c}$, Voigt $\vec{E} \parallel \vec{B}$	No

This is in complete agreement with the selection rules obtained in Sec. II C.

We also measured magnetotransmission of *circular* polarization in the Faraday geometry using samples cut perpendicular to the c axis ($\vec{q} \parallel \hat{c}$). In this case, EDSR is observed for the same sense of circular polarization as that which produces cyclotron resonance of *electrons*, and not for the opposite sense. This determines the sign of the g factor for the conduction band of $\text{Cd}_{1-x}\text{Mn}_x\text{Se}$ as *positive*. The determination of the sign of g_{eff} also constitutes a direct and unambiguous determination of the sign of the exchange constant α in Eq. (23), which governs the exchange interaction in the conduction band of wide-gap diluted magnetic semiconductors.¹⁴

The strength of EDSR increases with frequency, as can be clearly seen from the progression of observed resonance intensities for 251, 171, and 118.8 μm in Fig. 1. In Fig. 6 we plot the frequency dependence of the absorption strength (integrated intensity) $\alpha\Gamma$ obtained from the data for a sample with $x=0.10$ (ingot *B*) for two temperatures, $T=4.7$ and 9.8 K, where α is the absorption coefficient at the peak of EDSR, and Γ is the full width of the resonance at half maximum. The solid line of Fig. 6 shows the absorption strength $\alpha\Gamma$ calculated using Eq. (21). The

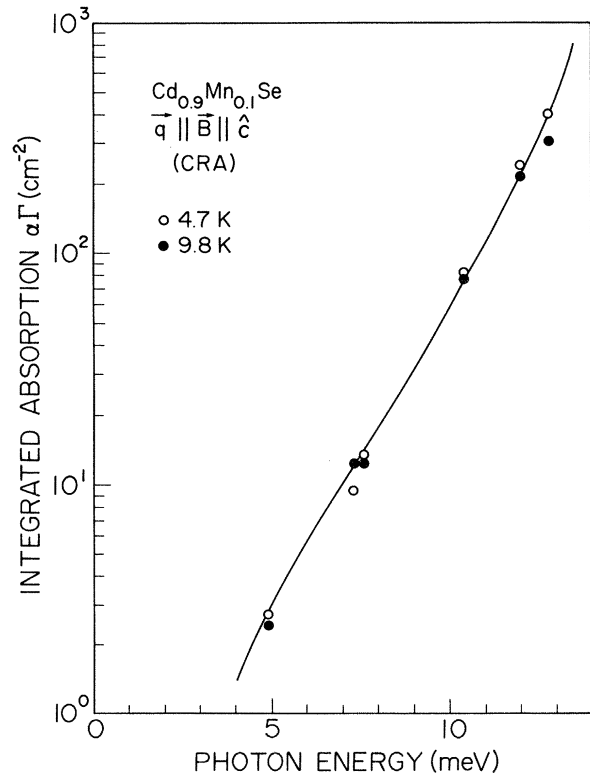


FIG. 6. Dependence of the integrated absorption $\alpha\Gamma$ for EDSR on the photon energy. Open and solid circles show experimental data obtained on $\text{Cd}_{0.9}\text{Mn}_{0.1}\text{Se}$ (ingot *B*) in the CRA polarization at 4.7 and 9.8 K, respectively. The solid curve is the best theoretical fit, obtained using Eq. (20) with $N=2.0 \times 10^{16} \text{ cm}^{-3}$, $\Delta E=15.5 \text{ eV}$, and $\lambda=6.05 \times 10^{-10} \text{ eV cm}$. (N is determined by Hall measurements; ΔE and λ are fitting parameters.)

good agreement between the observed sharp increase of EDSR intensity with frequency and the behavior predicted by Eq. (21) supports the validity of the theoretical model, and corroborates the assumption that the resonance observed at these low temperatures involves donor-bound electrons.

It is clear from Eq. (21) that when $\hbar\omega_s$ is not negligible relative to ΔE (as is the case in diluted magnetic semiconductors even at moderate magnetic fields), the frequency dependence of $\alpha\Gamma$ is highly sensitive to the value of ΔE . Taking $N=2\times 10^{16}$ cm $^{-3}$ (see Table I) and the index of refraction $n=3$, we obtain the best fit for all $x=0.1$ samples (ingots *A* and *B*) using $\lambda=6.05\times 10^{-10}$ eV cm and $\Delta E=15.5$ meV. The solid line in Fig. 6 shows the absorption strength calculated with these parameters. For the $x=0.2$ sample the best fit to the experimental data gives $\lambda=5.6\times 10^{-10}$ eV cm and $\Delta E=21$ meV. According to Romestain *et al.*,¹⁵ the parameter λ should scale as $\Delta/(m^*E_g^2)$, where Δ is the spin-orbit splitting and E_g is the energy gap. Since the ratio $E_g^2(x=0.2)/E_g^2(x=0.1)\simeq 1.16$ (Ref. 16), the above difference in λ appears reasonable. Both values of λ are of the same order of magnitude as the value of 1.6×10^{-10} eV cm for CdS.¹⁵ The value of this parameter is expected to be larger for CdSe because of the larger spin-orbit splitting in CdSe than in CdS. In the determination of λ the value of N (the number of occupied donors) is the largest uncertainty at this point. The estimate of N as equal to the room-temperature electron concentration (measured by the room-temperature Hall effect) should be accurate to within a factor of 2. Therefore the above values of λ should be viewed as having an uncertainty in accuracy of perhaps 30%.

The value of $\Delta E=15.5$ meV (found for samples with $x=0.1$) compares favorably with $E_{2p}-E_{1s}=\frac{3}{4}R^*=15$ meV (R^* is the effective Rydberg constant), estimated from the effective mass of the conduction band and the dielectric constant in pure CdSe.¹⁷ For the sample with $x=0.2$, a similar analysis of the data yields the value of $\Delta E=21$ meV. Arguing purely on the basis of the energy gaps corresponding to the $x=0.1$ and 0.2 samples, this increase of ΔE with x appears rather high (although it is qualitatively in the right direction). We should point out, however, that our $96.5\text{-}\mu\text{m}$ (12.8-meV) transmission experiments show a much stronger zero-field absorption for $x=0.1$ than for $x=0.2$, suggesting again that the value of ΔE is larger for the latter concentration, i.e., that for $x=0.2$ we are further away from $1s\rightarrow 2p$ transitions, as will be discussed below.

B. Magnetic-field-dependent background

It is clear from the observed spectra (see, e.g., Figs. 1, 2, and 4) that, in addition to EDSR, the magnetotransmission shows a magnetic-field-dependent background which also varies with frequency and temperature. This background has only been seen in the samples displaying EDSR, and not in the high-resistivity materials. Thus, although the purpose of this paper is to describe the spin-flip transition in $\text{Cd}_{1-x}\text{Mn}_x\text{Se}$, we shall briefly describe the variation of the overall spectrum, which appears to be

an inseparable companion feature of EDSR, and can probably be traced to the presence of donors.

There are three identifiable features in the observed background: low-frequency CRA absorption, which can be explained in terms of conduction-electron cyclotron resonance; high-frequency CRI absorption which we ascribe to the magnetic field dependence of the $1s\rightarrow 2p$ transition; and the sharp dip in transmission at low fields. We shall discuss them in turn.

1. Cyclotron resonance

As already mentioned, the broad dip in the $251\text{-}\mu\text{m}$ data at about 5 T in Fig. 1 can be explained as cyclotron resonance of conduction electrons. This interpretation is supported by measurements using circularly polarized light at $251\text{ }\mu\text{m}$, as shown in Fig. 7. The strong absorption line is observed only in the CRA polarization, and there is no trace of it in the opposite polarization. Measurements as a function of temperature show that, unlike EDSR, the position of cyclotron resonance shows no temperature variation, as would be expected for this transition.

The cyclotron-resonance interpretation implies that

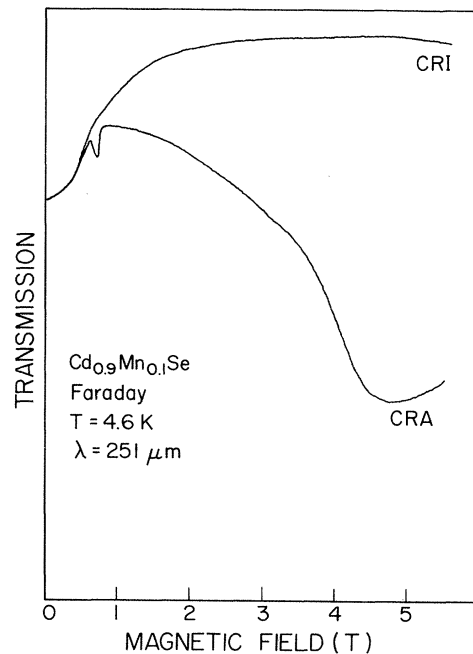


FIG. 7. Magnetotransmission in $\text{Cd}_{0.9}\text{Mn}_{0.1}\text{Se}$ in the Faraday geometry ($\vec{q} \parallel \vec{B} \parallel \hat{z}$, ingot *B*; same sample as in Fig. 6) at $251\text{ }\mu\text{m}$ at $T=4.6$ K for both circular polarizations. The broad CRA dip near 5 T is identified as cyclotron resonance. Note also that EDSR occurs only in the CRA circular polarization. The cyclotron resonance for this sample occurs at a slightly lower field than for ingot *A*; see Fig. 1. While we cannot account for this shift quantitatively, we point out that ingot *A* has a slightly higher value of x (see Table I), and that the data in Fig. 1 are obtained using unpolarized FIR. Either of these could contribute to a small relative shift of the transmission minimum between Figs. 1 and 7.

there are some free carriers in the conduction band at cryogenic temperatures. A possible explanation for the existence of free carriers has been given by Ichiguchi *et al.*¹⁸ Briefly, it is argued that local fluctuations of composition in the ternary compound $\text{Cd}_{1-x}\text{Mn}_x\text{Se}$ can lead to spatial fluctuations (on a submicrometer scale) of the energy gap. Fluctuations in x of 0.001 are not unreasonable, and this would correspond to local energy-gap fluctuations of the order of 20 meV. This is the ionization energy of the donors. With the chemical-potential constant on a macroscopic scale, it is not unreasonable to expect a small fraction of donor-bound electrons to "spill over" to the regions of lower-energy gaps. With $2 \times 10^{16} \text{ cm}^{-3}$ donors in the material, it is possible that about 0.5% of the donors are ionized in this manner. We recognize that this interpretation is highly conjectural. It is, however, the only mechanism that we can invoke to explain the strong CRA absorption systematically observed at the lower FIR frequencies.

Assuming that a fraction of the donors are ionized in this manner, cyclotron-resonance absorption in the Faraday geometry can be analyzed in terms of the dielectric response function

$$\epsilon_{\pm} = \epsilon_{\text{st}} - \frac{4\pi n_c e^2 / m^*}{\omega[(\omega \pm \omega_c) + i\tau^{-1}]}, \quad (26)$$

where the upper and lower signs refer to the two opposite senses of circular polarization, and ϵ_{st} is the static dielectric constant (which for pure CdSe equals 9.4, and should be close to that value for our sample¹⁷), n_c is the concentration of the free electrons, m^* is their effective mass, τ is the relaxation time, and $\omega_c = eB/m^*c$ is the cyclotron frequency.

We have used Eq. (26) to analyze the far-infrared transmission data, using n_c and τ as fitting parameters. The position of the cyclotron resonance, $\omega = \omega_c$, gives the value of the effective mass, $m^* = 0.12m_e$, in close agreement with the value $0.13m_e$ for CdSe.¹⁷ The best-fit curves are shown in Fig. 8 (dashed lines) for $n_c = 1.3 \times 10^{14} \text{ cm}^{-3}$ and $\hbar/\tau = 1.7 \text{ meV}$. The calculated spectrum is seen to agree well with the experimental trace above 10 kG. Below 10 kG the dielectric function given by Eq. (26) predicts a flat transmission spectrum (dashed curves in Fig. 8), while the experiments systematically display a dip, which must therefore be ascribed to a different mechanism (see below). We should add that the above relaxation time τ is about an order of magnitude longer than that obtained from the dc mobility ($\mu_n \approx 1800 \text{ cm}^2/\text{V sec}$ at 77 K, and expected to be considerably less at 4.6 K because of ionized-impurity scattering). This, however, does not weaken our assumption. In our model the carriers spill over to regions *away* from the ionized parent donors, i.e., precisely where their mobility would not be impeded by scattering on ionized impurities.

2. Tail absorption of the $1s \rightarrow 2p$ transition

As was shown in Fig. 7, at $251 \mu\text{m}$ the absorption of one sense of circular polarization can be explained in

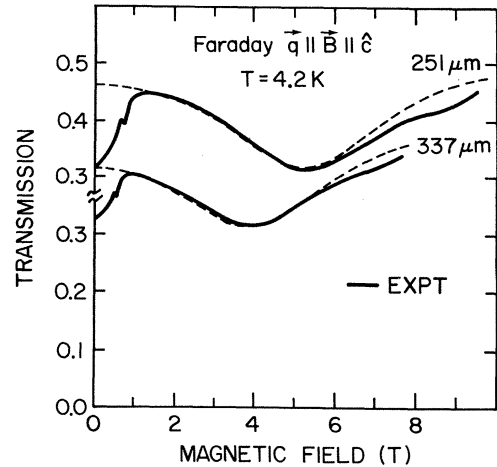


FIG. 8. Magnetotransmission in $\text{Cd}_{0.9}\text{Mn}_{0.1}\text{Se}$ at 4.2 K. The dashed line is the calculated transmission using the free-carrier dielectric function, Eq. (26), with $m^* = 0.125m_e$, $n_c = 1.3 \times 10^{14} \text{ cm}^{-3}$, and $\hbar/\tau = 1.7 \text{ meV}$.

terms of cyclotron resonance. This situation changes drastically at shorter wavelengths. Figure 9 presents the magnetotransmission spectra taken at $118.8 \mu\text{m}$ in the Faraday geometry for both circular polarizations. For this frequency the selective absorption of circular polarization is opposite, i.e., the CRA transmission (the one displaying EDSR) is *higher* than CRI. This behavior can be explained by the fact that, with increasing frequency,

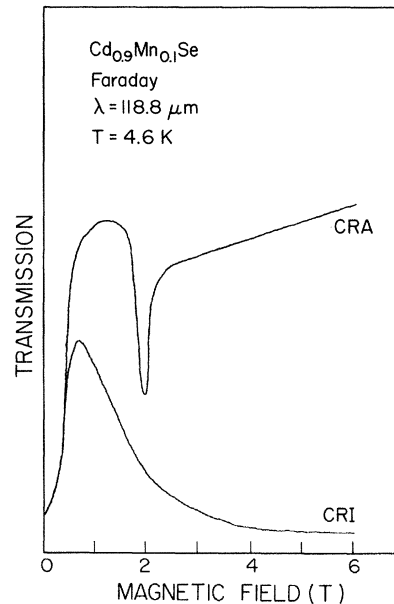


FIG. 9. Magnetotransmission in $\text{Cd}_{0.9}\text{Mn}_{0.1}\text{Se}$ (ingot B , $\vec{q} \parallel \vec{B} \parallel \hat{c}$; same sample as in Fig. 7) observed at $118.8 \mu\text{m}$ and $T = 4.6 \text{ K}$ for both circular polarizations. The EDSR is present only in the CRA polarization, as expected. Note, however, that in contrast to Fig. 7 the sample is now less transparent to CRI than to CRA at high fields, indicating the presence of a new, high-frequency absorption mechanism.

we approach the vicinity of the $1s \rightarrow 2p$ absorption (estimated earlier to occur at 15 meV at $B=0$), which eventually overshadows other mechanisms of absorption, and dominates the response of the sample at high fields.

The effect of the $1s \rightarrow 2p$ mechanism can be understood with the aid of Fig. 10. The inset of the figure shows a schematic diagram of the magnetic field dependence of $1s$, $2s$, and $2p$ states of a hydrogenlike donor. For clarity, we neglect the spin splitting of these states here, and we also ignore the higher excited states. In the presence of a magnetic field, the $2p$ hydrogenic state is split into three components, corresponding to the orbital angular momentum magnetic quantum numbers $m = +1, -1, 0$, and marked by superscripts $+$, $-$, and 0 , respectively. The electric-dipole selection rules for the $1s \rightarrow 2p$ transition are then

$$1s \rightarrow 2p^+(\Delta m = +1),$$

for the CRA polarization,

$$1s \rightarrow 2p^-(\Delta m = -1),$$

for the CRI polarization, and

$$1s \rightarrow 2p^0(\Delta m = 0),$$

for the $E \parallel \vec{B}$ polarization, with spin conserved.

The main body of Fig. 10 shows the energy dependence of the imaginary part of the dielectric constant ϵ'' in an applied dc magnetic field for CRA, CRI, and $\pi(E \parallel \vec{B})$ polarizations. The dashed vertical line in the figure indicates the energy of an incident photon in the vicinity of the $1s \rightarrow 2p$ transition. When the magnetic field intensity is increased, the energy of the $1s \rightarrow 2p^+$ transition in-

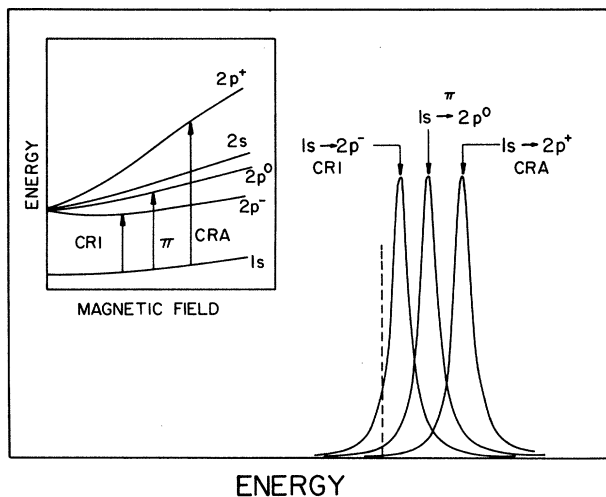


FIG. 10. Schematic presentation of the energy levels of a hydrogenlike donor in the presence of a magnetic field, and the resulting behavior of $1s \rightarrow 2p$ absorption. The inset shows the $1s$, $2s$, and $2p$ levels of the donor, with the arrows indicating the electric-dipole-allowed transitions between $1s$ and $2p$ levels for CRI, CRA, and parallel Voigt (π) polarizations. The main body of the figure shows the energy dependence of the absorption for each of these normal modes in a finite magnetic field. The dashed line indicates the energy of the incident FIR photon.

creases while the $1s \rightarrow 2p^-$ energy decreases. With the energy of the incident photon below the $1s \rightarrow 2p$ transition, the sample should then become more transparent to the CRA polarization, while for CRI polarization the transmission should strongly decrease.

In $\text{Cd}_{1-x}\text{Mn}_x\text{Se}$ the spin splitting of each level is much larger than the orbital m splitting. In this case the ground state is spin polarized at low temperatures, and the $1s \rightarrow 2p$ transitions can occur only between the spin-down levels. In this sense the situation in $\text{Cd}_{1-x}\text{Mn}_x\text{Se}$ is unique compared to a nonmagnetic semiconductor, but this does not alter the conclusions illustrated by Fig. 10.

The circular dichroism associated with selective absorption of the CRI polarization should become increasingly pronounced as the photon energy approaches the energy of the $1s \rightarrow 2p$ transition. The magnetotransmission spectrum in $\text{Cd}_{1-x}\text{Mn}_x\text{Se}$ ($x=0.1$) taken at $\lambda=96.5 \mu\text{m}$ ($E=12.8 \text{ meV}$) for both circular polarizations and for the parallel Voigt geometry is presented in Fig. 11. The transmission at zero magnetic field is already quite weak because of the proximity of the $1s \rightarrow 2p$ transition (estimated to be about 15 meV at $B=0$). As expected for the parallel Voigt geometry (the π polarization), the transmission remains at about a constant level—except in the very-low-field region, which is due to another interaction (see below), and near EDSR (about 2.4 T), which is allowed for this geometry. For CRI, on the other hand, the transmission drops even further (as the $1s \rightarrow 2p^-$ splitting decreases and approaches the incident-photon energy $\hbar\omega$ with increasing B), while for CRA it shoots up dramatically as the energy of the $1s \rightarrow 2p^+$ splitting moves away from $\hbar\omega$.

Figure 12 presents the magnetotransmission for $103 \mu\text{m}$ (12 meV) and $96.5 \mu\text{m}$ (12.8 meV), observed on the same sample as in Fig. 11, but with much lower sensitivity. Only transmission for the CRA polarization is shown in

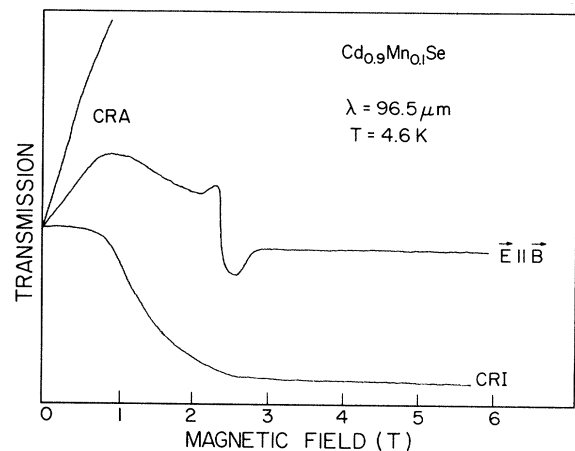


FIG. 11. Magnetotransmission in $\text{Cd}_{0.9}\text{Mn}_{0.1}\text{Se}$ (ingot B , c axis normal to sample face) at $96.5 \mu\text{m}$ for the Faraday (CRA and CRI), and for parallel Voigt ($E \parallel \vec{B}$) geometries. The “wiggle” in the $E \parallel \vec{B}$ is due to EDSR, which is allowed in this geometry, but not in CRI (see Table II). The same CRA data (here mostly off scale) are also shown in Fig. 12, with much lower gain.

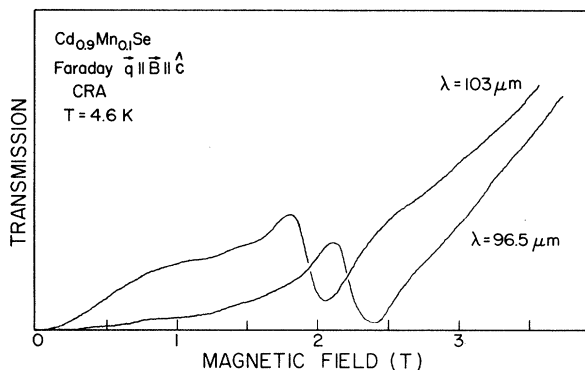


FIG. 12. CRA magnetotransmission in $\text{Cd}_{0.9}\text{Mn}_{0.1}\text{Se}$ (ingot *B*) observed at 96.5 and 103 μm at 4.6 K in the Faraday geometry, $\vec{q} \parallel \vec{B} \parallel \hat{c}$. The data are taken at a much lower gain than in Fig. 11 (at this gain, the CRI and Voigt signals shown in Fig. 11 would not be visible). The figure illustrates the fact that the effect of magnetic field is to “open” the sample to CRA transmission.

Fig. 12. On the scale of this figure the CRI and Voigt signals are practically indistinguishable from zero. It is indeed a fortunate coincidence that the CRA transmission (in which EDSR occurs) is the one which “opens up” as a function of B , thus making it possible to observe EDSR in samples which are opaque at $B=0$.

Although we cannot reach the $1s \rightarrow 2p$ energy with FIR energies available to us, we can use the dichroism just described as a source of information about the $1s \rightarrow 2p$ absorption line, i.e., the line shape and its width. We are presently attempting to analyze the dichroism data to obtain quantitative information about this transition.

3. Low-field background

In addition to the CRA absorption which we ascribe to cyclotron resonance, and the magnetic effects of the $1s \rightarrow 2p$ transition, all samples displaying EDSR also exhibit a striking dip in transmission at low fields. This low-field absorption is present in all polarizations, as can be seen in Figs. 7 and 9, and it becomes stronger with increasing frequency (Fig. 1). As a function of temperature, the width of the low-field dip appears to scale in a manner qualitatively similar to the EDSR field, as in Fig. 4, suggesting that the effect involves the magnetization or the effective g value. It is interesting to note that, in the pa-

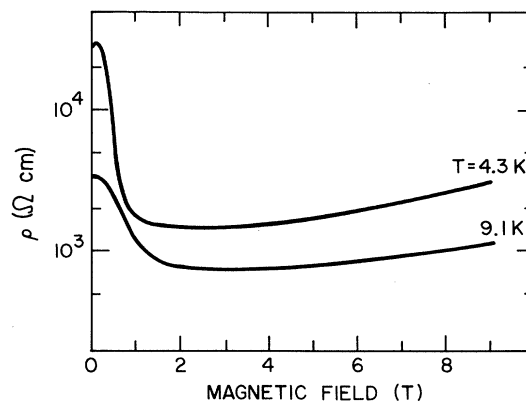


FIG. 13. Transverse magnetoresistance of $\text{Cd}_{0.9}\text{Mn}_{0.1}\text{Se}$ (ingot *A*) at 4.3 and 9.1 K.

rameter range in question (below 1 T at 4.2 K), $\text{Cd}_{1-x}\text{Mn}_x\text{Se}$ also displays strong anomalies in magnetoresistance, as illustrated in Fig. 13. Some of the present authors¹⁸ have suggested an interpretation of this low-field feature in terms of a condensation of the free carriers responsible for the cyclotron resonance into a D^- band at low magnetic fields (where D^- binding energy is larger than the Zeeman splitting). However, the physics of the impurity band for these donor densities ($a_0^* N_d^{1/3} \sim 0.1$)—especially for the unknown impurity and/or defect species involved—is rich with other possible interpretations. For this very reason the behavior of the transmission background described above (the low-field dip and the cyclotron resonance) are of great interest and deserve further systematic study.

ACKNOWLEDGMENTS

We wish to thank S. Rodriguez and S. Gopalan for valuable discussions, V. J. Goldman for use of his transport results prior to publication, and W. Gariat and H. R. Harrison for growing the excellent $\text{Cd}_{1-x}\text{Mn}_x\text{Se}$ crystals. This work was supported in part by the National Science Foundation (NSF) through Grant Nos. DMR-79-23310 and DMR-80-25017, and by the U. S. Office of Naval Research through Contract Nos. N00014-81-0654 and N00014-82-0563. We also acknowledge the use of the Purdue Central Materials Preparation Facility and Central Laser Facility, supported by NSF-MRL Grant No. DMR-80-20249.

*Present address: Institute of Physics of the Polish Academy of Sciences, 02-668 Warsaw, Poland.

†Present address: Institute of Experimental Physics, Warsaw University, 00-681 Warsaw, Poland.

¹A preliminary report on EDSR in $\text{Cd}_{1-x}\text{Mn}_x\text{Se}$ was published in M. Dobrowolska, H. D. Drew, J. K. Furdyna, T. Ichiguchi, A. Witowski, and P. A. Wolff, *Phys. Rev. Lett.* **49**, 845 (1982).

²R. C. Casella, *Phys. Rev. Lett.* **5**, 371 (1960).

³See, e.g., J. K. Furdyna, *J. Appl. Phys.* **53**, (11), 7637 (1982), and references cited therein.

⁴M. Nawrocki, R. Planel, G. Fishman, and R. R. Galazka, *Phys. Rev. Lett.* **46**, 735 (1981).

⁵D. Heimann, P. A. Wolff, and G. Warnock, *Phys. Rev. B* **27**, 4848 (1983).

⁶T. Dietl and J. Spalek, *Phys. Rev. B* **28**, 1548 (1983).

⁷Y. Yafet, in *Solid State Physics*, edited by F. Seitz and D. Turnbull (Academic, New York, 1963), Vol. 14, p. 1.

- ⁸V. I. Sheka, *Fiz. Tverd. Tela* **6**, 3099 (1964) [*Sov. Phys.—Solid State* **6**, 2470 (1965)].
- ⁹For the cubic structure, see E. I. Rashba and V. I. Sheka, *Fiz. Tverd. Tela (Leningrad)* **3**, 1735 (1961); **3**, 1863 (1961) [*Sov. Phys.—Solid State* **3**, 1257 (1961); **3**, 1357 (1961)]; M. H. Weiler, R. L. Aggarwal, and B. Lax, *Phys. Rev. B* **17**, 3269 (1978).
- ¹⁰For the wurtzite structure, E. I. Rashba and V. I. Sheka, *Fiz. Tverd. Tela (Leningrad)* **6**, 141 (1964) [*Sov. Phys.—Solid State* **6**, 114 (1964)].
- ¹¹J. R. Anderson (private communication).
- ¹²T. Dietl, in *Physics in High Magnetic Fields*, edited by S. Chikazumi and N. Miura (Springer, Berlin, 1981), p. 344.
- ¹³M. Dobrowolska, Y. F. Chen, J. K. Furdyna, and S. Rodriguez, *Phys. Rev. Lett.* **51**, 134 (1983).
- ¹⁴See, e.g., J. A. Gaj, *J. Phys. Soc. Jpn.* **49**, Suppl. A, 797 (1980).
- ¹⁵R. Romestain, S. Geschwind, and G. E. Devlin, *Phys. Rev. Lett.* **39**, 1583 (1977).
- ¹⁶P. Wisniewski and M. Nawrocki, *Phys. Status Solidi B* **117**, K43 (1983); see also M. Arciszewska and M. Nawrocki, in *Proceedings of the XIth Conference on the Physics of Semiconducting Compounds, Jaszowiec, Poland, 1981*, edited by J. M. Langer (Ossolineum, Warsaw, 1982), p. 225.
- ¹⁷H. H. Woodbury and M. Aven, *Phys. Rev. B* **9**, 5195 (1974).
- ¹⁸T. Ichiguchi, H. D. Drew, and J. K. Furdyna, *Phys. Rev. Lett.* **50**, 612 (1983).